2015 IEEE International Conference on Robotics and Automation (ICRA)
Washington State Convention Center
Seattle, Washington, May 26-30, 2015

Terrain Traversability Prediction by Imaging Thermal Transients

Chris Cunningham[1], Issa Nesnas[2], and William L. Whittaker[1]

Abstract— **The inability of current robotic perception techniques to adequately detect non-geometric terrain hazards is a primary cause of failure for robots operating in natural terrain on Mars, the Moon, and Earth. Classical approaches detect surface appearance but do not measure the underlying mechanical properties that determine wheel-terrain interaction. Diurnal temperature variations of a granular material, however, are strongly correlated with both its surface appearance and subsurface geophysical properties. This paper presents a technique for determining relative differences in looseness and traversability of granular terrain through analysis of thermal imagery. Terrain compaction and traversability are predicted by estimating a material's thermal inertia from observations of thermal transients. Results from a set of experiments in sandy terrain demonstrate the ability of this approach to differentiate between safe, compact and hazardous, loose terrain.**

I. Introduction

Mobile robots operating in natural terrain encounter loose, granular materials that can cause wheels to slip and sink, inhibiting mobility and sometimes even permanently trapping a vehicle. Looseness of granular terrain is difficult to predict using traditional sensing methods, such as cameras and LIDAR, that only see surface appearance and geometry but not the mechanical properties of a material. This paper presents a method for predicting the traversability of terrain by analyzing thermal imagery to provide a greater understanding of material properties both at and below the surface.

The ability to reliably predict the mobility properties of terrain is particularly important to rovers operating in planetary environments. On the Moon, the Apollo 15 Lunar Roving Vehicle spun its wheels and got stuck in loose regolith, requiring the astronauts to lift it out [1]. The Russian Lunokhod rovers experienced wheel sinkage of up to 20 cm [2]. On Mars, the Opportunity rover was trapped in the Purgatory Dune for five weeks in 2005 [3], and Spirit's mission came to an end when it fell through a thin crust on the surface, becoming permanently entrapped in the soft regolith underneath [4]. Even recently, Curiosity had to divert from its planned route after experiencing wheel slip of up to 80% [5]. More reliable prediction and avoidance of dangerous terrain would greatly improve the safety and efficiency of planetary rovers.

Portions of this research were carried out at the Jet Propulsion Laboratory, California Institute of Technology, under a contract with the National Aeronautics and Space Administration. Copyright 2014 California Institute of Technology. This work was supported by the NASA National Robotics Initiative program under contract NNX12AM05G as well as a NASA Space Technology Research Fellowship

[1]The Robotics Institute, Carnegie Mellon University ccunningham@cmu.edu, red@cmu.edu

[2]Jet Propulsion Laboratory, California Institute of Technology issa.a.nesnas@jpl.nasa.gov

Prior work on non-contact traversability prediction for robots operating in planetary environments has primarily centered on vision-based methods. Halatci et al. use color, texture, and depth from Mars Exploration Rover stereo imagery to classify terrain into different three traversability classes: rocky, sandy, and mixed [6]. Angelova et al. use similar visual features to predict wheel slip, achieving about 20% error when tested in soil, sand, gravel, and wood chips [7]. Although these vision-based techniques have achieved some success in relatively coarse terrain classes, they are fundamentally limited by only sensing the surface of a material. The appearance of the surface layer is not necessarily correlated with subsurface characteristics and does not provide enough information to fully understand all the physical properties of terrain that influence mobility, such as compaction and particle size.

However, diurnal temperature variations are not only influenced by the surface layer but also the physical properties of the material underneath. Terrain surface temperature is governed by a balance of heat fluxes from the sun, the atmosphere, and the subsurface. The thermal properties of a material and thus the subsurface heat flux are strongly influenced by the particle size, compaction, layering, and cementation of the material. This relationship has been used to infer geological composition at the global scale on both Earth and Mars from infrared imagery taken by orbiting satellites [8], [9], [10]. This analysis of orbital infrared imagery was used to help select landing sites for the Mars rover missions that were both safe and scientifically interesting [11].

Orbital thermal data is also used by mission planners when selecting long-term routes for the rovers. However, the resolution is far too low to detect rover-scale hazards. The Miniature Thermal Emission Spectrometer (Mini-TES) instruments aboard the Mars Explroation Rovers and the Ground Temperature Sensor (GTS) aboard Curiosity have been used to estimate the thermophysical properties of the Martian surface [12], [13]. These instruments, however, only give very sparse spatial coverage and are not used to inform day-to-day rover operations. Work has also been conducted on Earth using a laser to heat a material and infer thermophysical properties from the temperature response [14]. However, this method also has very limited spatial coverage.

This research develops a method for predicting the looseness of terrain by estimating its thermal inertia from observations of temperature over the course of a day. Thermal inertia is a property of a material that represents its resistance to changes in temperature. For a granular material, it is strongly influenced by particle size, compaction, and cementation, all of which also influence traversability. Estimated thermal

inertia is directly correlated with traversability and is used to minimize slip along a traverse. The efficacy of this method is highly dependent on the time of day of an observation as well as the length of an observation. Expected errors in thermal inertia estimates are computed as a function of the time and length of an observation to understand the practicality of this method. The efficacy of this method for predicting traversability as well as the validity of the predicted errors presented are evaluated through experiments in a sand pit.

The paper is organized as follows. Section II discusses background on the surface energy balance, thermal inertia, and connection to mobility. Section III presents the method for estimating thermal inertia and analyzes the expected error. Experiments are described in Section IV and their results are analyzed in Section V. Section VI discusses conclusions and directions for future research.

II. Background

Thermal inertia is a bulk property that governs a material's resistance to change in temperature due to periodic illumination. Thermal inertia is defined as $I = \sqrt{k\rho c}$ where k is thermal conductivity, ρ is bulk density, and c is specific heat capacity. The units of thermal inertia are $Jm^{-2}K^{-1}s^{-\frac{1}{2}}$ [15]. It is of particular importance when considering planetary terrain because it is a strong function of certain geophysical properties that also influence mobility, such as particle size, density, and cementation.

A. Surface Energy Balance

The temperature at the surface of a material is a balance between upwelling and downwelling fluxes from the Sun, the atmosphere, and the ground. The equation representing this surface boundary condition is:

$$(1-A)R_{sw} + \varepsilon R_{lw} - \varepsilon\sigma T_s^4 = H + LE - I\sqrt{\frac{\pi}{P}}\left.\frac{\partial T}{\partial Z}\right|_{Z=0} \quad (1)$$

A is albedo, ε is emissivity, σ is the Stefan–Boltzmann constant, P is the period of solar insolation (i.e. the length of a day), R_{sw} is the downwelling shortwave radiation from the Sun, R_{lw} is the downwelling longwave radiation from the Sun and the atmosphere, T_s is the temperature of the surface, and $\left.\frac{\partial T}{\partial Z}\right|_{Z=0}$ is the derivative of temperature in the ground evaluated at the surface. Finally, H and LE are the sensible and latent heat fluxes from the atmosphere, respectively.

R_{sw}, R_{lw}, H, and LE can be estimated using models for radiative and turbulent heat flux through the atmosphere. This is more easily done on Mars than Earth because H and LE are generally negligible and the atmospheric effects on the radiative terms are more easily predicted. On Earth, weather patterns and atmospheric effects make estimation of these fluxes more difficult. Given all other variables, T_s can be calculated over time by solving the 1D heat diffusion equation

$$\frac{\partial T}{\partial t} = \frac{k}{\rho c}\frac{\partial^2 T}{\partial Z^2} \quad (2)$$

with a surface boundary condition given by (1) and an insulating boundary condition at infinity. Though this equation is not a function of thermal inertia explicitly but instead a combination of conductivity, bulk density, and specific heat capacity, the temperature at the surface is only a function of conductivity, and nominal values of specific heat capacity and density can be assumed since they only effect the subsurface temperature profile [10]. For more detailed derivations see [15] and [16].

B. Thermal Inertia

In a granular material, thermal inertia is determined by three different mechanisms: the thermal conductivity of the contacts between grains, radiative heat transfer between grains, and gas conductivity in the voids between grains [15]. The thermal conductivity of the solid particles do not have a large effect on the the thermal inertia since the limiting factor in the solid path is the grain contacts [17]. The three heat transfer mechanisms that do have a large effect on thermal inertia are affected by particle size, cementation, and porosity. In general, more cemented, lower porosity, higher particle size materials have higher thermal inertias [18].

By far the dominant heat transfer mechanism is gas conduction in the spaces between grains. At Martian atmospheric pressure, this conductivity is a very strong function of particle size and porosity. On Earth, conductivity is still affected by particle size and porosity. However, their effects are not nearly as pronounced due to the higher terrestrial atmospheric pressure. This phenomenon is non-existent on the Moon due to vacuum. Consequently, the techniques discussed in this paper are tested on Earth but would perform better on Mars and significantly worse on the Moon. See [19] for an in depth discussion of thermal inertia.

C. Connection with Mobility

The traversability of an uncemented granular material is primarily governed by particle size distribution, particle shape, and density [20]. Particle size and shape distribution are principal parameters determining a material's range of strength while bulk and relative density modulate strength [21]. In general, larger particle sizes and higher densities correspond to higher traversability. In addition, as a granular material becomes more cemented through water and chemical processes, it generally becomes more traversable.

Because particle size, density, and cementation are primary factors in determining both traversability and thermal inertia, without a direct observation of particle size, density, and cementation, traversability and thermal inertia are correlated. Thus, an observation of thermal inertia can provide insight into the wheel-terrain interaction. This has been demonstrated experimentally for changes in density [14].

III. Methodology

For a given granular material, higher thermal inertia generally implies higher traversability. Relative differences in traversability are estimated using relative differences in thermal inertia. First, a method for estimating the thermal

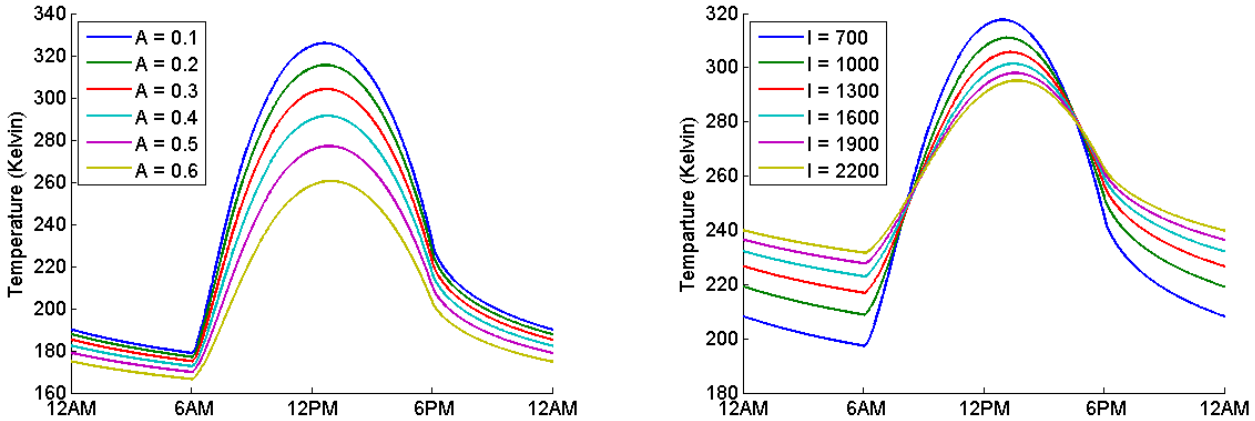

Fig. 1: Plots of analytical temperature curves showing the effect of varying albedo (left) and thermal inertia (right). Albedo values are dimensionless and thermal inertia values are given in $Jm^{-2}K^{-1}s^{-\frac{1}{2}}$.

inertia of terrain is presented. Then expected errors and limitations of the method are analyzed.

A. Thermal Inertia Estimation

Thermal inertia of terrain is estimated by observing its temperature with a thermal camera over a period of time, then fitting the resulting temperature curve to the analytical model described in Section II-A with estimated values for heat fluxes. This model is specialized to heat fluxes and measurements on Earth. However, similar analysis is even more applicable on Mars with more accurate models available since atmospheric effects are more predictable [22].

The heat fluxes in this work are time-varying and estimated using a mixture of ground truth measurements and statistical models. R_{sw} is measured directly using a pyranometer. R_{lw} is estimated as a function of air temperature and dew point using a statistical model for atmospheric radiation under clear skies [23]. LE is assumed to be zero, since all experiments were performed in a relatively dry climate. Finally, H is approximated as $\alpha(T_s - T_a)$, where T_a is air temperature and α is a constant that is learned by observing temperatures prior to data collection and finding the best-fit value.

Using these heat flux values and measured surface temperatures, thermal inertia is estimated by minimizing the root mean squared error between the measured and analytical surface temperatures with thermal inertia as a free variable. If surface temperature measurements are limited to a single point in time, then albedo is estimated by other means and kept as a fixed value in the optimization. However, for longer observation periods, albedo is also treated as a free variable in order to account for errors in the albedo estimate.

Thermal inertia estimates are sensitive to errors in heat fluxes. This makes comparing thermal inertia estimates with different start times and observation periods difficult since errors in the model fluctuate with time. However, when comparing temperature curves using the same model over the same period of time, these errors are less important and the relative differences in thermal inertia hold more reliably. This means that if one region's thermal inertia is estimated to be higher than another, its actual thermal inertia is higher. This can be exploited to maximize traversability over terrain by traveling on materials with higher relative thermal inertia.

B. Expected Error

The effects different parameters have on diurnal temperature variations of terrain are not constant over the course of a day. For example, Figure 1 shows temperature curves generated by the analytical thermal model for different values of albedo and thermal inertia. During the day, changes in albedo have a larger effect on temperature than at night, and changes in thermal inertia have a lower effect on temperature than at night. Understanding how errors in parameters affect thermal inertia estimates over the course of a day is critical for understanding the reliability of traversability prediction.

The two major sources of error considered here are in the estimation of albedo and of surface temperature. These are the two largest sources of error identified on the MER Mini-TES instruments. Other errors are caused by the estimation of H, LE, R_{sw}, and R_{lw}, but these effects are harder to quantify [13]. In order to analyze errors in temperature and albedo, first ground-truth temperature curves were created using the thermal model and reasonable values for all parameters, including a thermal inertia of 800 $Jm^{-2}K^{-1}s^{-\frac{1}{2}}$ and an albedo of 0.3. Then the method described in Section III-A was used to estimate the thermal inertia using incorrect values for temperature and albedo to see how those errors would affect the resulting thermal inertia value. The induced errors in albedo and temperature were derived from expected errors for the same values on the Mini-TES instruments in order to understand how well this technique could work on Mars. The maximum albedo error was assumed to be 0.02, and the maximum temperature error was assumed to 1K during the day and 3K at night. The temperature error was treated as an additive constant because the major source of temperature error is calibration, which results in a bias rather than noise [13]. Albedo error was not allowed to be a free parameter for either experiment.

The maximum thermal inertia error was computed at evenly spaced start times and observation periods by comparing the ground truth thermal inertia to estimated thermal

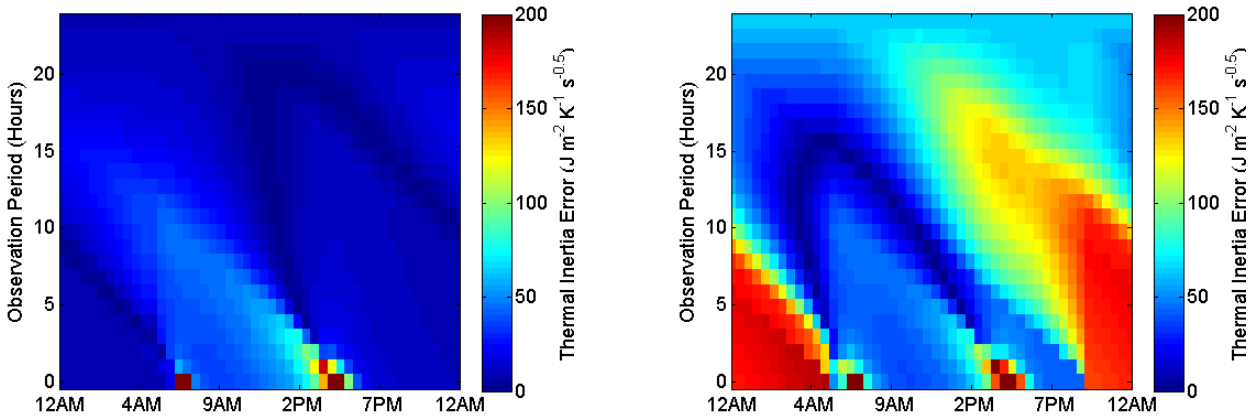

Fig. 2: The effect of errors in albedo (left) and temperature (right) on resulting thermal inertia estimates as a function of observation start time and observation period. Error is capped at 200 to prevent saturation of the colormap.

inertias. Start time is defined as time when the observation of temperatures begins. Observation period is defined as the length of time that temperature curve is observed. Periods ranging between one single observation to a full 24 hour period were considered. The error is plotted in Figure 2. In general, observing for longer periods of time produces a better estimate. The highest errors are for short observation periods in the morning when the terrain starts to heat up and in the evening when the terrain starts to cool down. This is supported by the graphs in Figure 1, which show that temperature curves with different thermal inertias intersect at those times. In the albedo analysis, there is higher error during the day and lower error at night, with the lowest error represented by a parabolic shape that occurs when moderate-length observations straddle the morning or the evening. In the temperature analysis, there is higher error at night than during the day, resulting from the higher uncertainty at night. Errors from a bias in temperature are of less concern in this application because relative differences in temperature between regions in the scene should hold.

IV. Experiments

Three experiments were conducted to validate the correlation between traversability and thermal inertia, the effects of time of day and length of observation, and the ability of thermal inertia to differentiate of different preparations of the same granular material. For each experiment, 15 different samples were prepared in a grid pattern in a sand pit. 8 cells of the grid were compacted and 7 were loosened. The compact samples were prepared by removing the surface layer of the sand to reveal a more compact, cemented layer of sand underneath. The loose samples were prepared by manually loosening with a shovel. Both classes were smoothed on the top layer to provide a similar visual appearance for all cells.

The experiments were conducted in July in Pasadena, CA. The sand was very dry, so it is assumed that LE was not an important factor. The sandpit was adjacent to several buildings and trees. These obstructions caused shadows on the sandpit during the day, which makes estimation of solar irradiance more difficult. The weather was mostly clear; however, there were short cloudy periods as well, which are not accounted for in the model for R_{lw}.

Infrared imagery was collected using a Thermoteknix Miricle 110K thermal camera, which is sensitive in the 8-12 μm spectral range. Because these cameras were not radiometrically calibrated and had high thermal drift, two blackbodies were placed in the field of view of the camera and held at different temperatures. Ground truth temperature of the blackbodies was measured throughout the day, with the exception of about 8 hours each night, to compensate for their fluctuating temperatures. By interpolating between the two temperature references in the the thermal images, temperature was estimated across the scene. Temperatures for the samples over time where calculated by manually selecting the regions in the thermal imagery and averaging the temperature within each region.

A pyranometer was placed next to the sand pit in order to get ground truth measurements for solar insolation. A DSLR viewed the scene to track the movement of shadows over the sand pit since the pyranometer is only a single point measurement. All instruments sampled at one minute intervals. The experimental setup is shown in Figure 3. Three datasets were collected with lengths: 48 hours, 15 hours, and 14 hours. For each data set, the α parameter for sensible heat flux was fit using the other two datasets. Shadows were

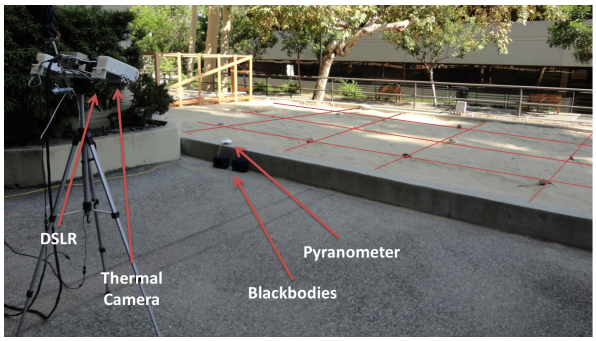

Fig. 3: The experimental setup showing the thermal camera and DSLR viewing a grid of compact and loose sand.

detected in the sand by first manually selecting the sand from the DSLR images. Then the images were converted to grayscale, and intensity values in the sandpit were fit to a mixture of Gaussians using variational inference [24]. Shadows were assigned to regions belonging to the lower-mean Gaussian.

Traversability of each sample was estimated by measuring wheel slip under a constant drawbar pull. The robot used in these measurements was an iRobot ATRV-JR, which weighs 50 kg and has pneumatic tires. For each test it was commanded forward at a constant velocity while a drag force of approximately 180 N was applied to the robot. A constant force was maintained by monitoring a spring scale. The velocity of the robot was measured by tracking three AprilTags on the side of the robot [25]. Wheel slip was calculated using difference between commanded and actual velocity divided by the commanded velocity, which was measured by driving on a flat, solid surface. However, there is some error in the slip measurements caused primarily by the variability in the robot's commanded velocity.

V. Results

The analytical model was fit to temperature and heat flux data to estimate thermal inertia for all 45 samples across the three datasets. When fitting to the full observation period of the sample, the average root mean squared error was 3.8 K with a maximum of 7.3 K and a minimum of 1.4 K. The model generally fit better to the samples in the datasets that had fewer clouds and fewer shadows. An example of the model fit to the data is shown in Figure 4.

For each of the three datasets, the estimated values for thermal inertia correlated strongly with the measured slip. Estimated thermal inertia is plotted against measured slip for the 48 hour dataset in Figure 5 where thermal inertia was estimated using the full 48 hour observation period. Despite some overlap between thermal inertias of the high-slip and low-slip samples, the five samples with the highest thermal inertia all have low slip values. Thus the behavior of driving on the terrain with the highest thermal inertia would result in low wheel slip. The loose and compact sample classes correlated well with the resulting slip and thermal inertia values despite intraclass variation due to the heterogeneity of the sandpit and errors in thermal inertia and slip estimation. This shows that thermal inertia can distinguish between different compactions of a granular material.

To show both the general applicability of this method along with its limitations, thermal inertia was estimated over the three datasets at different start times and for different observation periods. For purposes of analysis, it is assumed that samples with slip below 30% are traversable and sample with slip above 30% are not. The metric used to evaluate error is the percentage of traversable samples that have lower thermal inertia than the non-traversable sample with the highest thermal inertia. A lower error percentage implies that thermal inertia estimates have more correctly separated high-slip from low-slip samples. An error of 100% implies that

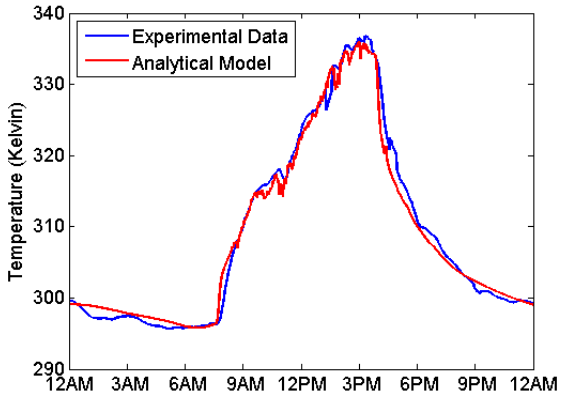

Fig. 4: Best-fit analytical model plotted with experimental data for a 24 hour period from the 48 hour dataset.

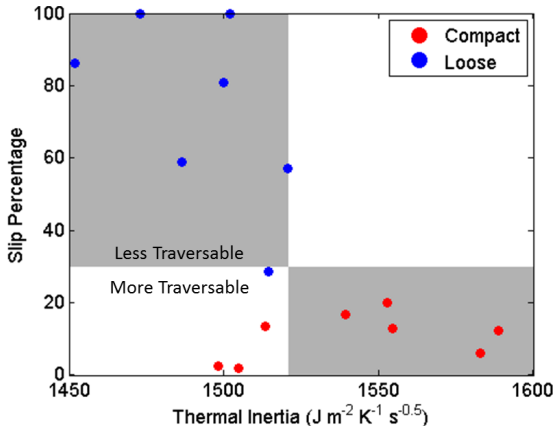

Fig. 5: Estimated thermal inertia plotted against measured slip for the 48 hour dataset. Thermal inertia was estimated using the entire observation period. The gray regions represent correct predictions assuming a decision boundary at the highest thermal inertia sample with slip higher than 30%.

the behavior of preferring to drive on the highest thermal inertia sample has failed.

The error metric was averaged over the three datasets. The results from this analysis are shown in Figure 6. The method only failed on 8% of the trials. In all others, the prescribed behavior of selecting the highest thermal inertia sample would have low-slip. The lowest error percentages were found with long observation periods and during the evening and night. The highest errors were found in samples that included data from the middle of the day during times when solar irradiance and surface temperature were not changing very quickly. These errors were likely due to errors in albedo and errors in estimated solar irradiance due to shadows. The parabolic shape of minimal error from the albedo error plot in Figure 2 is also evident in the the experimental data. This suggests that error in albedo estimation is a primary source of error. There were also higher errors with shorter observation periods at night likely due to errors in temperature estimation caused by the gap in periodic measurement of the blackbody temperatures during

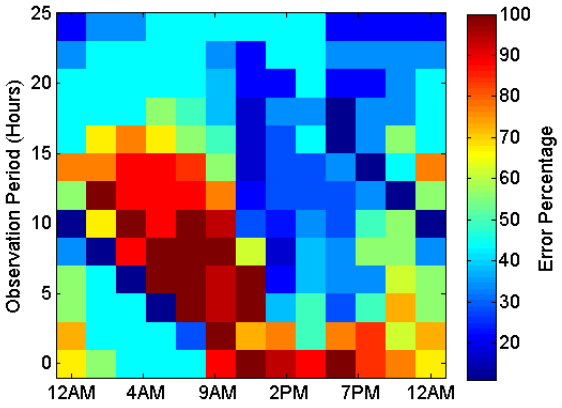

Fig. 6: Error in traversability prediction as a function of observation start time and observation period. The error metric is the percentage of samples with measured slip below 30% that have lower thermal inertia than the highest thermal inertia sample with slip above 30%.

the night. This agrees with the temperature error analysis in Figure 2, which shows that higher temperature uncertainty causes higher error.

VI. Conclusions

This paper presented a method for determining relative differences in traversability in granular materials by estimating thermal inertia from infrared imagery. Thermal inertia can differentiate between different compactions of the same material despite similar surface appearance. In general, higher thermal inertia granular materials are more traversable than lower thermal inertia granular materials. The quality of thermal inertia estimates and the resulting prediction of mobility is a function of both the length of time and time of day the terrain is observed. Longer observation periods and nighttime measurements generally lead to better estimates. A set of experiments modulating compaction in sand and measuring temperatures over several days supported the analysis of the expected error. These are promising preliminary results. However, further testing is needed with larger sample sets and more accurate traversability measurements.

One of the major practical limitations of this technique is that long observation periods are required to obtain a good prediction. Future work will investigate methods for shortening the required observation period to enable real-time operation. Current thermal inertia estimates are not consistent across time because of errors in estimating heat fluxes. Heat flux models must be improved to effectively capture the influences of the atmosphere. The exploitation of relative temperature differences between regions of terrains could also help create more consistent estimates of thermal inertia by providing additional constraints. Work to date has focused on detecting differences in compaction within the same material. Future work will analyze the efficacy of this technique when looking at different materials and different particle sizes and shapes. Finally, thermal analysis will be combined with visual-based learning techniques to learn models of the terrain and predict traversability.

References

[1] N. C. Costes, J. E. Farmer, and E. B. George, "Mobility Performance of the Lunar Roving Vehicle: Terrestrial Studies - Apollo 15 Results," no. December, 1972.

[2] D. A. Kring, "Lunar Mobility Review," in *Space Sciences*, 2006

[3] R. C., "Oppurtunity rolls out of Purgatory," *Science News*, vol. 167, no. 26, p. 413, 2005.

[4] J. Matson, "Unfree Spirit: NASA's Mars Rover Appears Stuck for Good," *Scientific American*, vol. 302, no. 16, 2010.

[5] J. Algar, "Curiosity rover forced to take road less traveled due to sand ripples," *Tech Times*, 2014

[6] I. Halatci, C. a. Brooks, and K. Iagnemma, "Terrain Classification and Classifier Fusion for Planetary Exploration Rovers," *2007 IEEE Aerospace Conference*, pp. 1–11, 2007

[7] A. Angelova, L. Matthies, D. Helmick, and P. Perona, "Learning and prediction of slip from visual information," *Journal of Field Robotics*, vol. 24, no. 3, pp. 205–231, 2007

[8] J. C. Price, "Thermal inertia mapping: A new view of the Earth," *Journal of Geophysical Research*, vol. 82, no. 18, pp. 2582–2590, June 1977

[9] R. L. Fergason, P. R. Christensen, and H. H. Kieffer, "High-resolution thermal inertia derived from the Thermal Emission Imaging System (THEMIS): Thermal model and applications," *Journal of Geophysical Research*, vol. 111, no. E12, p. E12004, Dec. 2006

[10] M. T. Mellon, B. M. Jakosky, H. H. Kieffer, and P. R. Christensen, "High-Resolution Thermal Inertia Mapping from the Mars Global Surveyor Thermal Emission Spectrometer," *Icarus*, vol. 148, no. 2, pp. 437–455, Dec. 2000

[11] M. Golombek, *et al.*, "Selection of the Mars Science Laboratory Landing Site," *Space Science Reviews*, vol. 170, no. 1-4, pp. 641–737, July 2012

[12] V. Hamilton, *et al.*, "Observations and preliminary science results from the first 100 sols of MSL Rover Environmental Monitoring Station ground temperature sensor measurements at Gale," *Journal of Geophysical Research: Planets*, pp. 745–770, 2014

[13] R. L. Fergason, *et al.*, "Physical properties of the Mars Exploration Rover landing sites as inferred from Mini-TESderived thermal inertia," *Journal of Geophysical Research*, vol. 111, no. E2, p. E02S21, 2006

[14] C. Cunningham, U. Wong, K. M. Peterson, and W. L. R. Whittaker, "Predicting Terrain Traversability from Thermal Diffusivity," in *Field and Service Robotics*, Brisbane, Australia, 2013.

[15] N. E. Putzig, "Thermal inertia and surface heterogeneity on Mars," Ph.D. dissertation, University of Colorado, 2006

[16] J. C. Price, "On the analysis of thermal infrared imagery: The limited utility of apparent thermal inertia," *Remote Sensing of Environment*, vol. 18, no. 1, pp. 59–73, Aug. 1985

[17] B. M. Jakosky, "On the thermal properties of Martian fines," *Icarus*, vol. 66, no. 1, pp. 117–124, Apr. 1986

[18] S. Piqueux and P. R. Christensen, "A model of thermal conductivity for planetary soils: 2. Theory for cemented soils," *Journal of Geophysical Research*, vol. 114, no. E9, p. E09006, Sept. 2009

[19] S. Piqueux and P. R. Christensen, "A model of thermal conductivity for planetary soils: 1. Theory for unconsolidated soils," *Journal of Geophysical Research*, vol. 114, no. E9, p. E09005, Sept. 2009

[20] D. Carrier, "The four things you need to know about the geotechnical properties of lunar soil," *Lunar Geotechnical Institute*, no. September, 2005

[21] W. Li, Y. Huang, Y. Cui, S. Dong, and J. Wang, "Trafficability analysis of lunar mare terrain by means of the discrete element method for wheeled rover locomotion," *Journal of Terramechanics*, vol. 47, no. 3, pp. 161–172, June 2010

[22] H. H. Kieffer, "Thermal model for analysis of Mars infrared mapping," *Journal of Geophysical Research: Planets*, vol. 118, no. 3, pp. 451–470, Mar. 2013

[23] S. B. Idso, "A Set of Equations for Full Spectrum and 8- to 14- um and 10.5- to 12.5-um Thermal Radiation From Cloudless Skies," *Water Resources Research*, vol. 17, no. 2, pp. 295–304, 1981.

[24] C. M. Bishop, *Pattern Recognition and Machine Learning*, 2006, vol. 4

[25] E. Olson, "AprilTag: A robust and flexible visual fiducial system," *2011 IEEE International Conference on Robotics and Automation*, pp. 3400–3407, May 2011